Acta Materialia 153 (2018) 108–116

Contents lists available at ScienceDirect

Acta Materialia

journal homepage: www.elsevier.com/locate/actamat

Full length article

Grain growth kinetics in submicrometer-scale molecular dynamics simulation

Shin Okita [a], Eisuke Miyoshi [b], Shinji Sakane [b], Tomohiro Takaki [c], Munekazu Ohno [d], Yasushi Shibuta [a, *]

[a] Department of Materials Engineering, The University of Tokyo, 7-3-1 Hongo, Bunkyo-ku, Tokyo, 113-8656, Japan
[b] Graduate School of Science and Technology, Kyoto Institute of Technology, Matsugasaki, Sakyo-ku, Kyoto, 606-8585, Japan
[c] Faculty of Mechanical Engineering, Kyoto Institute of Technology, Matsugasaki, Sakyo-ku, Kyoto, 606-8585, Japan
[d] Division of Materials Science and Engineering, Faculty of Engineering, Hokkaido University, Kita 13 Nishi 8, Kita-ku, Sapporo, Hokkaido, 060-8628, Japan

ARTICLE INFO

Article history:
Received 14 March 2018
Received in revised form
23 April 2018
Accepted 24 April 2018
Available online 27 April 2018

Keywords:
Molecular dynamics simulations
Grain growth
Nucleation
Solidification
Large-scale simulation

ABSTRACT

Grain growth kinetics under the anisotropic grain boundary properties is investigated by large-scale and long-time molecular dynamics (MD) simulations of contentious processes of nucleation, solidification and grain growth in a submicrometer-scale system. Microstructures obtained via homogeneous nucleation from undercooled melt iron consists of approximately 1500 grains and the number of grains decreases to one tenth of the number via the grain growth process. The grain growth exponent obtained from the MD simulation deviates from the ideal value since anisotropic effects in the grain boundary properties are inherently included in MD simulations. It is confirmed that the decrease of the reduced mobility (i.e., the product of the intrinsic grain boundary mobility and the grain boundary energy) is a dominant factor for the deviation from the ideal grain growth. The deviation from the Mackenzie function for the distribution of the disorientation angle between neighboring grains implies that the preferential selection of grain boundaries with small grain boundary energies occurs during the grain growth. This enhances the anisotropy in grain boundary properties and therefore decreases the reduced mobility of the grain boundary. Moreover, a multi-phase-field simulation starting from a MD configuration results in an ideal grain growth when a constant value of the reduced mobility is employed, which validates the discussion on the reduced mobility. The new insight in this study is achieved for the first time owing to a multi-graphics processing unit (GPU) parallel computation over 50 days for one case using 128 GPUs on the GPU-rich supercomputer.

1. Introduction

Microstructure is an essential ingredient of metallic materials since the microstructure strongly affects properties of the product [1,2]. The manufacturing of metallic materials involves many thermal control processes, in which the grain growth is a key phenomenon to determine the size and morphology of microstructure. Therefore, it is essential to control the grain growth process to obtain designed products. Since it is not straightforward to reveal the kinetic aspects of grain growth from experimental observation in general, numerical simulations have contributed to the understanding of fundamental aspects of grain growth [3–20]. For example, Monte Carlo (MC) simulations based on the Potts model [3] have been widely carried out to study the grain growth kinetics [4–6]. Moreover, cellular automata (CA) [7–9], a front tracking method [10,11], a level set model [12] and a vertex model [13] are often used for the grain growth kinetics from the mesoscale point of view. Recently, a phase-field (PF) model becomes a mainstream of studies of grain growth kinetics [14–20] since it is not necessary in the PF model to explicitly track the position of grain boundaries in the polycrystalline microstructure. Combined with the recent rapid progress in high-performance computational environments [21–23], an ultra-large-scale PF simulation with more than three million grains now reaches a complete steady-state behavior in the ideal grain growth [24].

Although the PF simulation is a very powerful tool, there are some remaining problems in the PF model for the grain growth kinetics. One of the problems is the inclusion of anisotropic effects

* Corresponding author.
E-mail address: shibuta@material.t.u-tokyo.ac.jp (Y. Shibuta).

https://doi.org/10.1016/j.actamat.2018.04.060
1359-6454/

in the grain boundary properties. At present, most of PF simulations employ simple approximations such as Read-Shockley relation [25] for the anisotropy in the grain boundary energy and a sigmoidal relation [26] for that in the grain boundary mobility, which are approximation models for low-angle grain boundaries. However, it is not straightforward for the multi-phase-field (MPF) model to reproduce prominent energy cusps at high-angle grain boundaries [27–29] since the original MPF model [14] becomes numerically unstable where energies of the grain boundaries adjoining a triple junction exhibit large differences [19,20]. In order to overcome this problem, special treatments such as higher-order models [19,20,30] and a specific model connecting a database [31] are needed. As a second problem of PF simulations is how to treat the nucleation event since it requires the development of a reliable statistical model for nucleation or modeling of fluctuation of state variables triggering the nucleation. Therefore, nuclei in the melt are specified in advance as under some specific rule, which causes the artificial initial configuration of the grain growth simulation in most cases.

On the other hand, anisotropic effects in the grain boundary energy [27–29,32,33] and the grain boundary mobility [33–35] are inherently included in MD and other atomistic simulations since the atomistic configuration determines the grain boundary properties. In addition, it is possible in principle to achieve a thermally-activated nucleation without any inducing factor in the MD simulation if a spatiotemporal scale is sufficiently large. Recent large-scale MD simulations successfully achieved the multiple nucleation from the undercooled melt, which was followed by the formation of polycrystalline microstructures [36–40]. Especially, we have investigated the cutting-edge parallel computing technique using graphics processing units (GPUs), which drastically increases the spatiotemporal scale of the MD simulation [40]. In particular, a billion-atom MD simulation performed on the GPU-rich supercomputer produced a fine microstructure consisting of approximately 35000 grains [40]. The morphology of the microstructure obtained from the MD simulation is much more realistic than that from analytical Laguerre-Voronoi tessellation [41,42] since the microstructure from the MD simulation is formed via nucleation and solidification as in the case of the experimental process. Moreover, a grain growth process has been investigated by long-time MD simulations of annealing of the MD-generated microstructure [37,43,44] and a grain growth kinetics in the MD simulations is directly compared with analytical models such as the von Neumann-Mullins law for a two-dimensional system [45,46] and the MacPherson–Srolovitz model for a three-dimensional system [47].

Most of the MD studies on grain growth kinetics showed a large deviation from the ideal grain growth even in the pure element [43,44]. Although many reasons have been proposed for the deviation from the ideal grain growth such as the shortage of number of grains, the transition state before reaching a steady state growth and the anisotropic effect in grain boundary properties, the physical origin of the deviation from the ideal grain growth is not well investigated from the atomistic point of view mainly due to the computational limitation except for the pioneering work [48]. As described above, we have successfully performed large-scale MD simulations with up to a billion atoms on the GPU-rich supercomputer before the times [37,38,40]. By utilizing this cutting-edge multi-GPU computational technique, the origin of deviation from the ideal grain growth is closely investigated by large-scale and long-time MD simulations.

2. Simulation methodology

The simulation methodology basically follows previous studies [38,40]. The Finnis–Sinclair (FS) potential [49] is employed for the interatomic potential between iron atoms, which is one of the most established potentials for body-centered-cubic (bcc) metals. The total energy of the FS potential, E, is expressed as follows:

$$E = \frac{1}{2}\sum_i \sum_j V_{ij}(r_{ij}) - A\sum_i \sqrt{\rho_i} \tag{1}$$

$$V_{ij}(r_{ij}) = \begin{cases} (r_{ij}-c)^2\left(c_0 + c_1 r_{ij} + c_2 r_{ij}^2\right) & (r_{ij} \le c) \\ 0 & (r_{ij} > c) \end{cases} \tag{2}$$

$$\rho_i = \sum_{j \ne i} \varphi(r_{ij}) \tag{3}$$

$$\varphi(r_{ij}) = \begin{cases} (r_{ij}-d)^2 + \beta\dfrac{(r_{ij}-d)^3}{d} & (r_{ij} \le d) \\ 0 & (r_{ij} > d) \end{cases}, \tag{4}$$

where V is the repulsive term, r_{ij} is the bond length between atoms i and j, ρ is the total electronic charge density at the site of atom i, which is constructed by the rigid superposition of atomic charge densities ϕ, A is the binding energy, c_0, c_1, and c_2 are the free parameters used for fitting experimental data, c and d are cutoff parameters assumed to lie between the second-nearest- and third-nearest-neighbor atoms, β is a parameter used to introduce a maximum value of ϕ within the first-nearest-neighbor distance. The parameters for bcc iron from the original FS paper are employed [49] (Table 1). A leapfrog method is used to integrate the classical equation of motion with a time step of 5.0 fs. The Berendsen thermostat [50] is applied to control the temperature in each step, and the Andersen method [51] is applied to independently control the pressure in each direction.

Fig. 1 shows the initial configuration of the calculation system, which is prepared by heating a bcc crystal of iron of size 110.2 × 110.2 × 110.2 nm (384 × 384 × 384 unit cells, 113, 246, 208 atoms) at 3000 K with the constant-NVT ensemble. The prepared initial configuration is annealed isothermally in the main calculation for 30,000 ps (6,000,000 steps) under zero pressure with the constant-NPT ensemble at 1400 K. Since the melting point of bcc iron given by the FS potential is $T_m = 2400$ K [28], which is higher than the experimental value of 1811 K, temperatures normalized by T_m are employed. That is, 1400 K correspond to 0.58 T_m. Calculations with the same temperature are performed twice using different initial configurations to confirm the reproducibility of the simulation. Hereafter, results from two independent calculations are named 1 s t and 2nd calculations, respectively.

After the MD simulations, the obtained atomic configurations are first analyzed by common neighbor analysis (CNA) to identify solid and liquid structures [40,52]. The atoms with the bcc configuration are determined by considering the coordination numbers of the first- and second-nearest-neighbor atoms using two cutoff lengths (see Ref. [52] for more technical information). Next, the disorientation angle relative to the coordination axis is estimated for all atoms with the bcc configuration. Then, neighboring atoms with a difference in the crystal orientation of less than 3° are classified as belonging to the same grain. The average disorientation angle for all atoms in the grain is regarded as the disorientation

Table 1
Potential parameters of iron for the Finnis-Sinclair potential employed in the simulation [49].

d [Å]	A [eV]	β	c [Å]	c_0	c_1	c_2
3.569745	1.828905	1.8	3.40	1.2371147	−0.3592185	−0.0385607

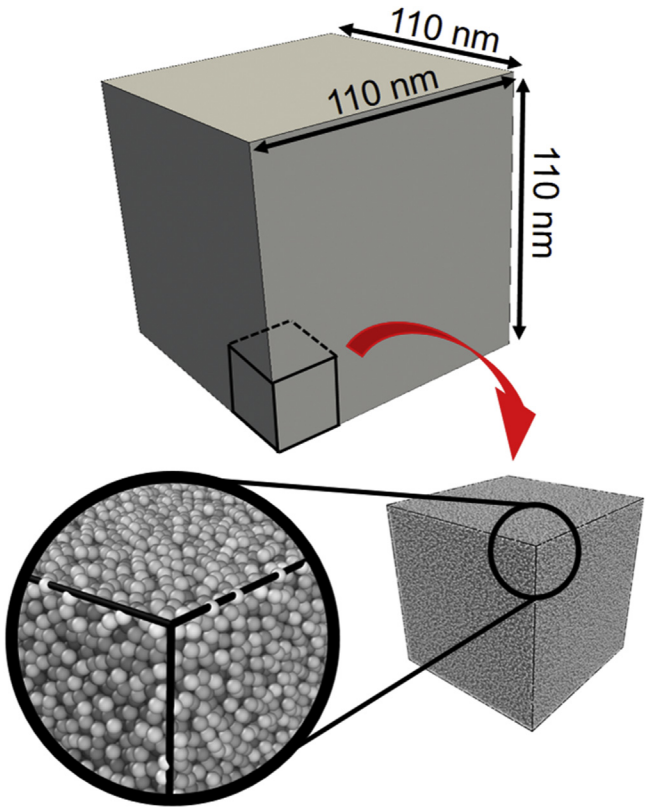

Fig. 1. Initial configuration of the simulation cell filled with iron melt. The system consists of 113, 246, 208 atoms in a cell of $110.2 \times 110.2 \times 110.2\ nm^3$ with the periodic boundary condition.

angle of the grain. All atoms are colored in accordance with the disorientation angle of the grain in the range from 0° to 62.80° [40,53]. The volume of each grain, V is estimated by the summation of atomic volumes of all atoms in the grain and the radius of the grain, r is estimated assuming the grain is spherical as $r = \sqrt[3]{3V/4\pi}$.

All computations are performed on the GPU-rich supercomputer TSUBAME2.5 at the Tokyo Institute of Technology with an original parallel GPU code [40] developed with the Compute Unified Device Architecture (CUDA) and the Message Passing Interface (MPI) for internode communication. The technical detail of the parallel GPU computation is shown in Refs. [23, 40]. The whole simulation cell is divided into subdomains and each subdomain is assigned to one GPU. The domain decomposition method [54,55] is also applied to accelerate the search for neighboring atoms in each subdomain. The whole domain is divided into 128 ($1 \times 8 \times 16$) subdomains, and therefore 128 GPUs (NVIDIA K20X) are parallelized for the MD simulations. Using 128 GPUs, approximately 600 ps calculation (300,000 MD steps) proceeds per day. Therefore, a run time for 30,000 ps (i.e., 6,000,000 MD steps) calculation with 128 GPUs was about 50 days for one calculation. Therefore, it totally took about 100 days using 128 GPUs for two independent calculations. Post-analyses (i.e., CNA, determination of disorientation angle and so on) are also performed on the GPU supercomputer.

3. Results and discussion

3.1. Atomic configuration and grain growth exponent for grain growth in MD simulations

Fig. 2 shows snapshots of simulation cells during 30000 ps for two independent calculations. All grains larger than 1.0 nm are colored in accordance with the disorientation angle relative to the coordination axis and the area of the liquid is colored in white. As a whole, there is no significant difference between two independent calculations. In both cases, many small grains appear at 100 ps and they grow larger with time. Solidification is almost completed and almost all the spaces are filled with many grains having various orientations by 500 ps. After that, small grains disappear and lager ones become larger during the relaxation at the same temperature until 30000 ps, which is regarded as the grain growth process. Fig. 3 shows the number of grains as a function of time. Approximately 1500 grains exist just after the solidification at 500 ps for both calculations. The number of grains decreases drastically at the initial stage and becomes approximately 300 at 10000 ps, respectively. Then, it keeps deceasing monotonically and finally approximately 150 grains remain in the microstructures after 30000 ps calculation for both calculations. Since there is no significant difference in the time change of the number of grains for two independent calculations, it is confirmed that the system size is large enough to ensure the reproducibility of the calculation for the grain growth kinetics.

It is well known that the kinetics of the ideal grain growth follows a parabolic law [56,57]:

$$< r(t) >^2 - < r(t_0) >^2 = m \cdot (t - t_0), \quad m = KM\sigma \tag{5}$$

where t_0 is an initial time, K is the kinetic coefficient, M is the intrinsic grain boundary mobility and σ is the grain boundary energy. Fig. 4(a) shows the square of average grain radius as a function of time for the two simulations. The relationship is almost proportional only at the initial stage less than 5000 ps. Lines in the figure are fitted to the plots less than 5000 ps. After 5000 ps, the plots deviate from the fitted lines, which represents a non-ideal grain growth. In general, the grain growth kinetics might deviate from the parabolic law when grain growth does not reach the steady state [58]. Therefore, the kinetics of the grain growth is generally expressed as:

$$< r(t) >^n - < r(t_0) >^n = A \cdot (t - t_0) \tag{6}$$

where n is the grain growth exponent and A is the proportional constant. The grain growth exponent n becomes larger than 2 in the case of the non-ideal grain growth. Fig. 4(b) shows the average grain radius as a function of time for two simulations. From the fitted curve to Equation (6) with $t_0 = 500$ ps, grain growth exponents for two calculations are estimated to be 3.152 and 3.883, respectively. Actually, there are many reports on deviated values of the grain growth exponent by Monte-Carlo [4,6] and phase-field simulations [59] under the anisotropic conditions. Therefore, it is natural to obtain higher values of the grain growth exponent from the MD simulations.

3.2. Determination factors for the deviation from ideal grain growth

The product value, $m = KM\sigma$ of equation (5) can be defined by the slope of the tangent lines at each time of the simulation. Since the slope of the tangent lines decreases with time, it is expected that product value $KM\sigma$ should decrease. However, it is still unknown which factor in $KM\sigma$ causes the decrease of the product value, that is, the deviation from the ideal grain growth.

According to the Hillert's theory [56], the kinetic coefficient K is expressed as

$$K = \frac{2\alpha\rho^2}{\gamma}, \tag{7}$$

where α is a geometrical constant and ρ is a parameter determined

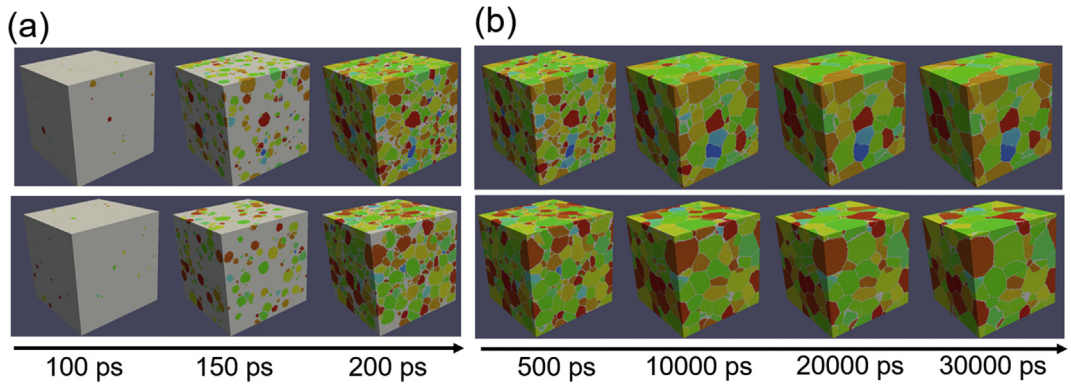

Fig. 2. Snapshots of simulation cells for (a) initial nucleation, solidification and (b) subsequent grain growth for two independent calculations of 30000 ps. All grains larger than 1.0 nm are colored in accordance with the disorientation angle relative to the coordination axis and the area of the liquid is colored in white.

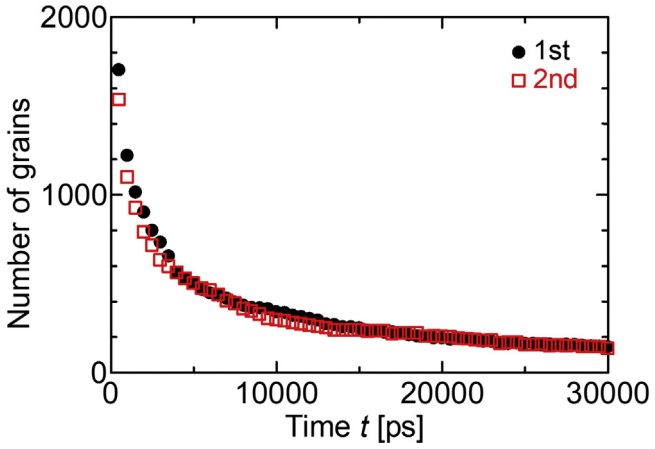

Fig. 3. Number of grains as a function of time for two independent calculations.

from the volume conservation as

$$\rho = \frac{<r>^2}{<r^2>}. \tag{8}$$

The value γ is a dependent variable of ρ and it can be defined using the following relation [60,61].

$$\rho \approx 0.8557 + 0.0107\gamma - 0.5509\exp(-\gamma) \tag{9}$$

Therefore, determination factors of the slope of equation (5), m are M, σ, α and ρ.

Here, the physical origin of the decrease of the grain growth exponent is closely examined by focusing on the time change of determination factors estimated from the MD simulations. Fig. 5 shows ρ as a function of time, which is directly calculated from the results of MD simulations. It is confirmed that the value ρ is almost constant in time, around 0.7, during the grain growth for both calculations. In turn, the value γ is estimated from Equation (9), which is also almost constant around 1.4. Therefore, there is no significant change in the values ρ and γ during the grain growth process. Next, the geometric constant, α is estimated using following relations. That is, the growth rate of individual grains is defined from the Hillert's mean field theory [56] as

$$r\frac{dr}{dt} = \alpha M\sigma\left(\rho\frac{r}{<r>} - 1\right) \tag{10}$$

Moreover, the topological equation for the growth kinetics for

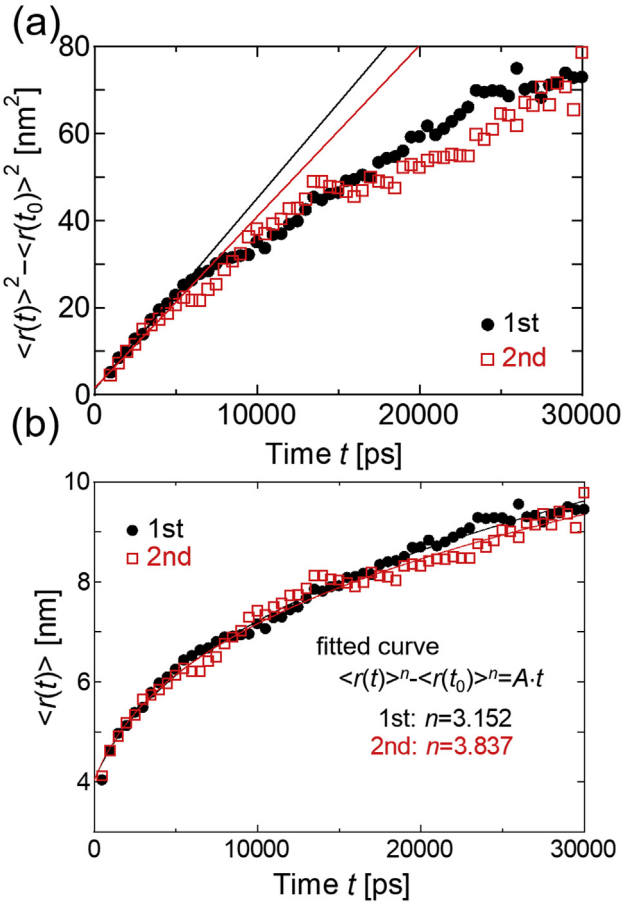

Fig. 4. (A) Squared average grain size as a function of time and (b) averaged grain size as a function of time for two independent simulations ($t_0 = 500$ ps). Plots in (b) are fitted to Equation (6) to estimate the grain growth exponent, n.

three-dimensional individual grains is derived in our previous study [43] as

$$\frac{dV}{dt} = 2\pi r M\sigma\left(\frac{\pi\sqrt{N}}{3} - 4\right), \tag{11}$$

where V is the volume of the grain and N is the number of neighboring grains. Using the relation $r = \sqrt[3]{3V/4\pi}$, Equation (11) is

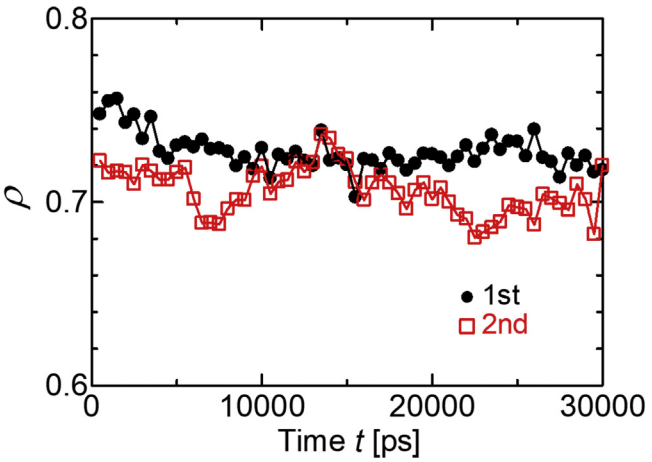

Fig. 5. The value ρ as a function of time calculated estimated from the MD simulations.

rewritten as

$$r\frac{dr}{dt} = M\sigma\left(\frac{\pi\sqrt{N}}{6} - 2\right). \tag{12}$$

From Equations (10) and (12), the geometric constant, α can be estimated from the slope of the following equation

$$\sqrt{N} = \alpha\frac{6}{\pi}\left(\rho\frac{r}{<r>} - 1\right) + \frac{12}{\pi}. \tag{13}$$

Fig. 6(a) shows the relationship in Equation (13) for several representative times from the 1 s t MD simulation. The geometric constant α can be estimated from the slope of the fitted line. In the same manner, the time change in the geometric constant, α is derived and summarized in Fig. 6(b). It is confirmed from the figure that the value of the geometric constant, α does not decrease but keeps the same level around 1.2 with some fluctuation.

Finally, the product of the intrinsic grain boundary mobility, M and the grain boundary energy, σ (called the reduced mobility) is estimated from the slope of Equation (11). Fig. 7(a) shows the relationship in Equation (11) for several representative times from the 1 s t MD simulation. The reduced mobility, $M\sigma$ can be estimated from the slope of the fitted line [43]. The reduced mobility as a function of time is summarized in Fig. 7(b). The reduced mobility apparently decreases in time for both calculations although there is some fluctuation to some extent. The value of reduced mobility becomes approximately one third of the initial value after 30000 ps. As a summary of analyses of determination factors, the reduced mobility, $M\sigma$ decreases in time during the MD simulation of the grain growth whereas there is no significant change in the value ρ and the geometric constant, α. Therefore, it is concluded that the decrease of the reduced mobility, $M\sigma$ causes the deviation from the ideal grain growth for the grain growth kinetics in the MD simulations.

3.3. Disorientation angle between neighboring grains during grain growth

The main advantage of MD simulations compared to PF simulations is that anisotropic effects of the grain boundary are inherently included in the simulation, whereas some artificial rule of the interface must be given for the PF simulations. However, it is not straightforward to extract these interfacial properties including the anisotropy in the polycrystalline system directly from the MD simulation although these interfacial properties should determine the main rule of the grain growth. Previously, Holm and Foiles [48] discussed the origin of grain-growth stagnation model based on the MD simulation of the pure metal. They concluded that the increase of the smooth (and slow) boundary with respect to the rough (and fast) boundary can stop the grain growth. As they stated in the literature [48], it is not feasible to measure the mobility of grain boundaries in a polycrystalline system, in which the driving force is poorly characterized and continually changing. Moreover, they also pointed out that geometric roughness is an inherently noisy measurement and the noise often obscures the signal of the roughening transition. Therefore, it is not straightforward to directly measure the reduced mobility for each grain boundary in the polycrystalline microstructure during the grain growth in the MD simulation at present.

Alternatively, we focus on the time change in the disorientation angle between neighboring grains to discuss the decrease in the reduced mobility. Fig. 8 shows the distribution of the disorientation angle between neighboring grains during the grain growth. The dashed line is the Mackenzie distribution function [53], which represents a random orientation. Just after the solidification completes at 500 ps, distribution of disorientation angle basically follows the Mackenzie distribution except for a peak near 60°. It agrees with our previous simulation of the homogeneous nucleation from undercooled iron melt [40]. That is, abundant coherent twin boundaries with an extremely small grain boundary energy appeared during the nucleation stage, which caused a peak near 60° [40]. As the grain growth proceeds, mismatch from the Mackenzie distribution around 60° becomes larger and the deviation from the random disorientation becomes prominent. This means that grain boundaries with small grain boundary energy tend to survive through the grain growth processes. Therefore, a preferential selection of grain boundaries with small grain boundary energies causes the decrease of the average grain boundary energy in the polycrystalline structure and therefore it causes the decrease of the reduced mobility. However, it is not enough to explain the reduction of reduced mobility by a factor three only from the change of the grain boundary energy. It is reasonable to consider that there is also a contribution from a change of the intrinsic grain boundary mobility. Although the intrinsic grain boundary mobility is affected by a changed disorientation angle, the change in the driving force should also affect the intrinsic grain boundary mobility. Recent atomistic simulations [62,63] demonstrate there are two different (i.e., diffusional and ballistic) modes in the intrinsic grain boundary mobility depending on the temperature and the driving force. Therefore, it is considered that the strong nonlinearity of the intrinsic grain boundary mobility depending on the driving force could contribute the reduction of the reduced mobility by a factor three. The intrinsic grain boundary mobility in the polycrystalline microstructure will be investigated in the next step.

3.4. Multi-phase-field simulation with isotropic boundary condition

Finally, the phase-field simulation is performed to validate the effect of decrease of the reduced mobility on the grain growth kinetics. Recently, we proposed a novel methodology to bridge atomistic and continuum-based simulations [64], in which the atomistic configuration from the MD simulation is converted into the interfacial profiles of the PF model. Using this technique, the MPF simulation starting from the microstructure obtained from the MD simulation is performed. In particular, the atomistic configuration at 12000 ps of the 1 s t MD simulation is converted into the interfacial profile for the MPF simulation and a MPF simulation is performed until 30000 ps with an isotropic interfacial condition to show the grain growth without the anisotropic interfacial effect.

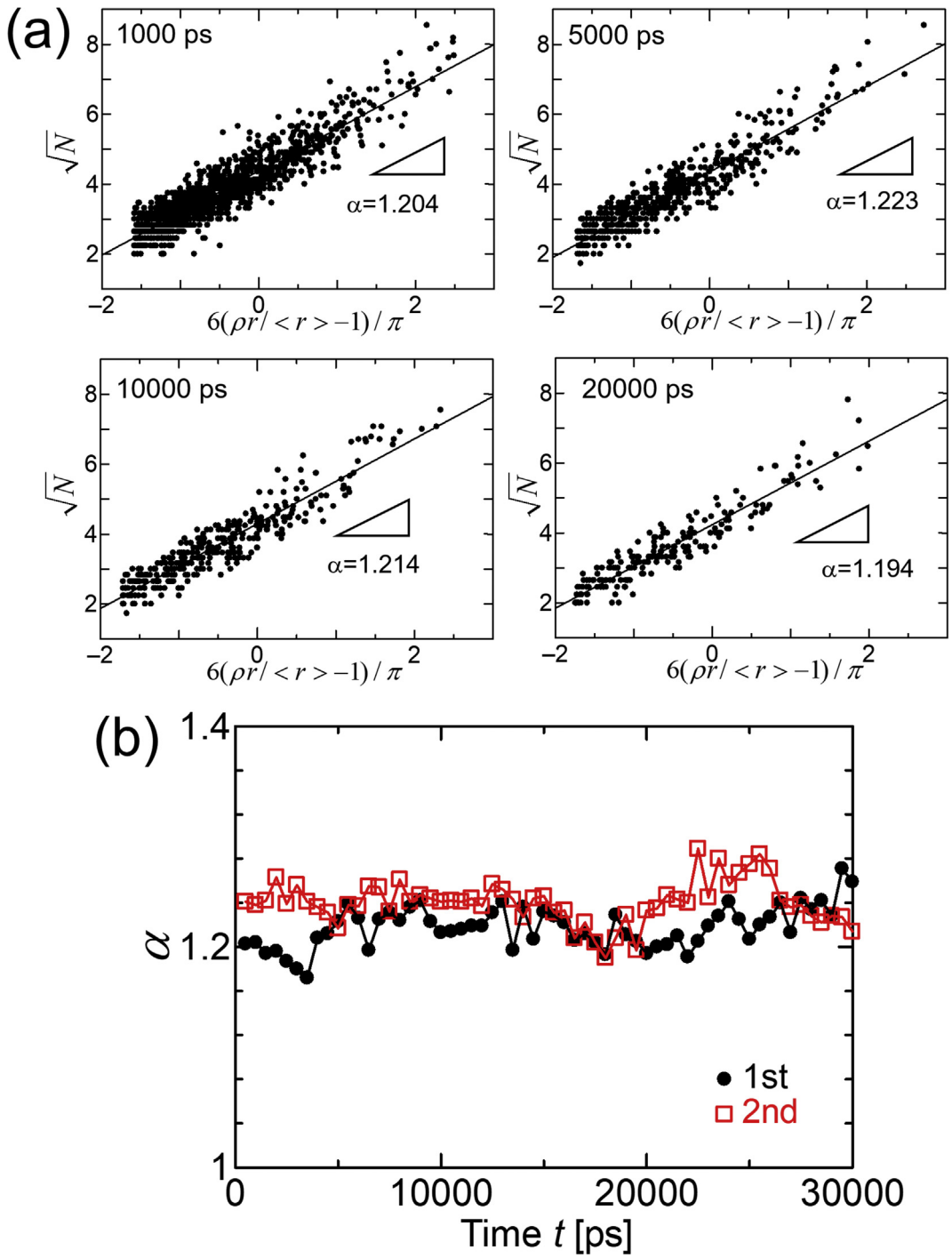

Fig. 6. (A) Relationship in Equation (13) for several representative times of the 1 s t MD simulation. The geometric constant, α can be estimated from the slope of the fitted line. (b) The geometric constant, α as a function of time for two independent calculations.

Here, the computational domain for the MPF simulation is divided into $432 \times 432 \times 432$ square regular grids with a size of $\Delta x = 0.25509$ nm. The grain boundary width, δ, is set to $6\Delta x$, and the time increment, Δt, to 0.5 ps. A constant value, 6.34×10^{-9} $m^2 s^{-1}$ is employed for the reduced mobility, $M\sigma$, which is derived from our previous MD study [43]. The technical detail of the MPF simulation is shown in our previous studies [24]. Fig. 9(a) shows snapshots of the MPF simulation starting from the configuration at 12000 ps of the 1 s t MD simulation. The squared average grain radius as a function of time for the MPF simulations is shown in Fig. 9(b). Since the average grain size is proportional to the time, it is confirmed that the ideal grain growth occurs in the MPF simulation with the isotropic condition, whereas the grain growth exponent of the corresponding the MD simulation is larger than 2 as shown in Fig. 4(b). Therefore, it is confirmed that the decrease of the reduced mobility surely causes the deviation from the ideal grain growth.

4. Conclusions

Most of MD studies on the grain growth kinetic showed a large

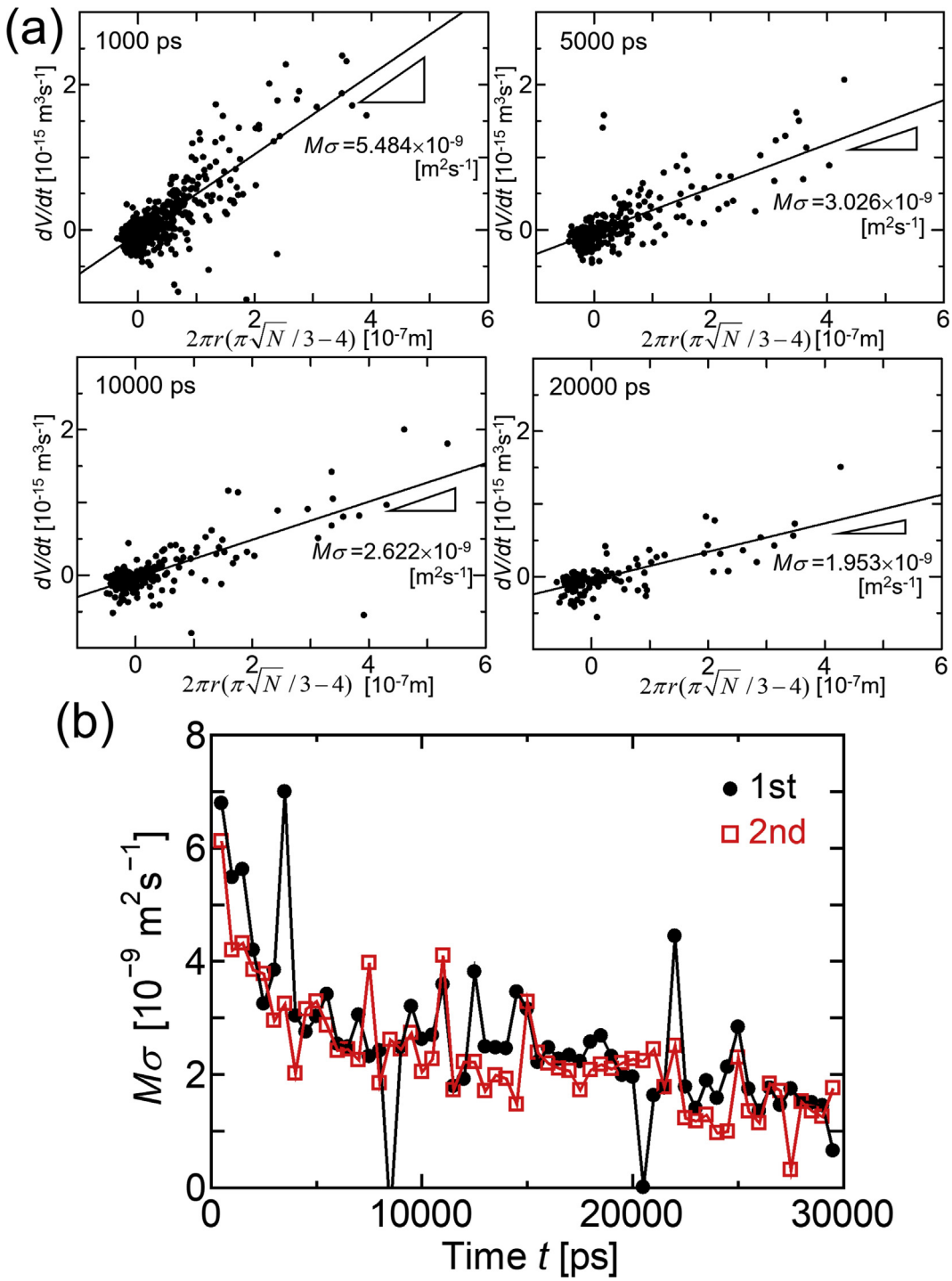

Fig. 7. (A) Relationship in Equation (11) for several representative times of the 1 s t MD simulation. The reduced mobility, $M\rho$ can be estimated from the slope of the fitted line. (b) The reduced mobility, $M\rho$ as a function of time for two dependent calculations.

deviation from the ideal grain growth even in the pure element. In this study, the physical origin of the deviation from the ideal grain growth is investigated by performing large-scale and long-time MD simulations at the submicrometer-scale. Although the geometric constant keeps constant during the grain growth, the reduced mobility drastically decreased over time. One of the reasons for the decrease is considered to be a preferential selection of grain boundaries with a small grain boundary energy, which is revealed by a change over time of the distribution of disorientation angle between neighboring grains. Moreover, the grain growth by the MPF simulation with the isotropic grain condition (i.e., the constant reduced mobility) starting from the MD configuration follows the parabolic law, which means the ideal grain growth appears in the MPF simulation. Therefore, it is concluded that the deviation from the ideal grain growth in the MD simulation is mainly caused by the anisotropic effect in grain boundary properties rather than the kinetic factor.

It is significant in this study to shed light on the determinant

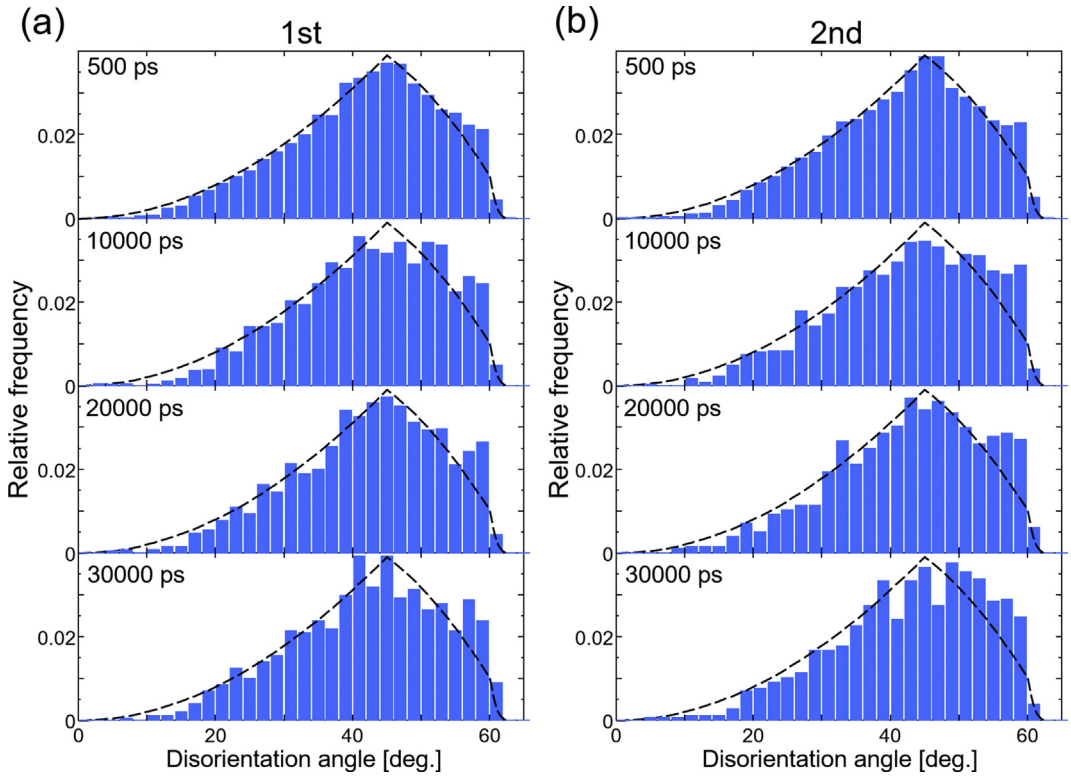

Fig. 8. Distribution of the disorientation angle between neighboring grains during the grain growth over 30000 ps. The dashed line is the Mackenzie distribution function [53], which represents a random orientation.

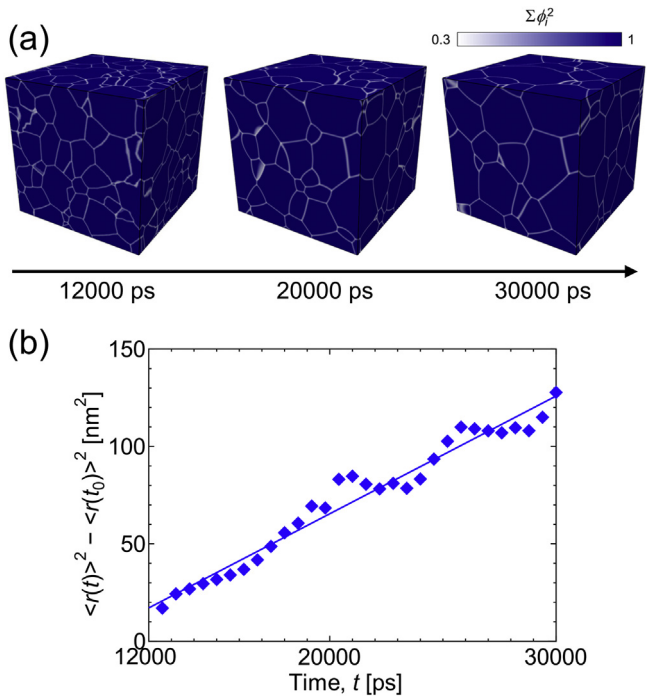

Fig. 9. (A) Snapshots of the multi-phase-field (MPF) simulation starting from the configuration at 12000 ps of the 1 s t MD simulation. (b) Squared average grain radius as a function of time for the MPF simulation ($t_0 = 12000$ ps).

factor of the deviation from the ideal grain growth by way of the large-scale MD simulation at the submicrometer-scale. Such progress is achieved for the first time owing to the multi-GPU parallel computation combined with the rapid progress in high-performance computational environments. Actually, the MD simulation over 30000 ps (6,000,000 steps) with more than hundred-million atoms, which takes about 50 days for one case even with 128 GPU parallel computing, is the toughest MD simulation to the best of our knowledge at present. On the other hand, it is not straightforward to define the Miller index of each grain boundary in the three-dimensional polycrystalline microstructure since the grain boundary of the three-dimensional polycrystalline microstructure is not simply planar structure. In addition, geometric roughness in the interface makes the measurement difficult. The systematic determination of the grain boundary in the complex three-dimensional polycrystalline structure will be investigated in the next step.

Acknowledgements

This work was supported by Grant-in-Aid for Scientific Research (A) (No.17H01237) and Grant-in-Aid for Scientific Research (B) (No.16H04490, 16H04541) from Japan Society for the Promotion of Science, Japan. This work was partially supported by the Joint Usage/Research Center for Interdisciplinary Large-scale Information Infrastructures (JHPCN) and the High Performance Computing Infrastructure (HPCI) in Japan for the computational environment. This work was also supported in part by MEXT as a social and scientific priority issue (creation of new functional devices and high-performance materials to support next-generation industries; CDMSI) to be tackled using the post-K computer.

References

[1] F.J. Humphreys, M. Hatherly, Recrystallization and Related Annealing Phenomena, second ed, Elsevier, Oxford, 2004.

[2] J.A. Dantzig, M. Rappaz, Solidification, EPFL Press, Lausanne, 2009.
[3] R.B. Potts, Some generalized order-disorder transformations, Math. Proc. 48 (1952) 106–109.
[4] D.J. Srolovitz, M.P. Anderson, G.S. Grest, P.S. Sahni, Grain growth in two dimensions, Scripta Metall. 17 (1983) 241–246.
[5] M.P. Anderson, D.J. Srolovitz, G.S. Grest, P.S. Sahni, Computer simulation of grain growth – I. Kinetics, Acta Metall. 32 (1984) 783–791.
[6] G.S. Grest, D.J. Srolovitz, M.P. Anderson, Computer simulation of grain growth – IV. Anisotropic grain boundary energy, Acta Metall. 33 (1985) 509–520.
[7] H.W. Hesselbarth, I.R. Göbel, Simulation of recrystallization by cellular automata, Acta Metall. Mater. 39 (1991) 2135–2143.
[8] M. Rappaz, C.A. Gandin, Probabilistic modelling of microstructure formation in solidification processes, Acta Metall. Mater. 41 (1993) 345–360.
[9] C.A. Gandin, M. Rappaz, A coupled finite element-cellular automaton model for the prediction of dendritic grain structures in solidification processes, Acta Metall. Mater. 42 (1994) 2233–2246.
[10] A. Jacot, M. Rappaz, A pseudo-front tracking technique for the modelling of solidification microstructures in multi-component alloys, Acta Mater. 50 (2002) 1909–1926.
[11] E.A. Lazar, J.K. Mason, R.D. MacPherson, D.J. Srolovitz, A more accurate three-dimensional grain growth algorithm, Acta Mater. 59 (2011) 6837.
[12] H. Hallberg, Influence of anisotropic grain boundary properties on the evolution of grain boundary character distribution during grain growth—a 2D level set study, Model. Simulat. Mater. Sci. Eng. 22 (2014) 085005.
[13] A. Vondrous, M. Reichardt, B. Nestler, Growth rate distributions for regular two-dimensional grains with Read–Shockley grain boundary energy, Model. Simulat. Mater. Sci. Eng. 22 (2014) 025014.
[14] I. Steinbach, F. Pezzolla, A generalized field method for multiphase transformations using interface fields, Physica D 134 (1999) 385–393.
[15] C.E. Krill III, L.-Q. Chen, Computer simulation of 3-D grain growth using a phase-field model, Acta Mater. 50 (2002) 3057–3073.
[16] S.G. Kim, D.I. Kim, W.T. Kim, Y.B. Park, Computer simulations of two-dimensional and three-dimensional ideal grain growth, Phys. Rev. E 74 (2006) 061605.
[17] Y. Suwa, Y. Saito, H. Onodera, Three-dimensional phase field simulation of the effect of anisotropy in grain-boundary mobility on growth kinetics and morphology of grain structure, Comput. Mater. Sci. 40 (2007) 40–50.
[18] R. Darvishi Kamachali, I. Steinbach, 3-D phase-field simulation of grain growth: topological analysis versus mean-field approximations, Acta Mater. 60 (2012) 2719–2728.
[19] E. Miyoshi, T. Takaki, Validation of a novel higher-order multi-phase-field model for grain-growth simulations using anisotropic grain-boundary properties, Comput. Mater. Sci. 112 (2016) 44–51.
[20] E. Miyoshi, T. Takaki, Extended higher-order multi-phase-field model for three-dimensional anisotropic-grain-growth simulations, Comput. Mater. Sci. 120 (2016) 77–83.
[21] T. Shimokawabe, T. Aoki, T. Takaki, A. Yamanaka, A. Nukada, T. Endo, N. Maruyama, S. Matsuoka, Peta-scale phase-field simulation for dendritic solidification on the TSUBAME 2.0 supercomputer, in: Proceedings of 2011 International Conference for High Performance Computing, Networking, Storage and Analysis, 2011, pp. 1–11.
[22] Y. Shibuta, M. Ohno, T. Takaki, Solidification in a supercomputer: from crystal nuclei to dendrite assemblages, JOM 67 (2015) 1793–1804. https://link.springer.com/article/10.1007%2Fs11837-015-1452-2.
[23] S. Sakane, T. Takaki, R. Rojas, M. Ohno, Y. Shibuta, T. Shimokawabe, T. Aoki, Multi-GPUs parallel computation of dendrite growth in forced convection using the phase-field-lattice Boltzmann model, J. Cryst. Growth 474 (2017) 154–159.
[24] E. Miyoshi, T. Takaki, M. Ohno, Y. Shibuta, S. Sakane, T. Shimokawabe, T. Aoki, Ultra-large-scale phase-field simulation study of ideal grain growth, npj Comp, Materials 3 (2017) 25.
[25] W.T. Read, W. Shockley, Dislocation models of crystal grain boundaries, Phys. Rev. 78 (1950) 275–289.
[26] F.J. Humphreys, A unified theory of recovery, recrystallization and grain growth, based on the stability and growth of cellular microstructures—I. The basic model, Acta Mater. 45 (1997) 4231–4240.
[27] D. Wolf, Correlation between the energy and structure of grain boundaries in b.c.c. metals. II. Symmetrical tilt boundaries, Philos. Mag. a 62 (1990) 447–464.
[28] Y. Shibuta, S. Takamoto, T. Suzuki, A molecular dynamics study of the energy and structure of the symmetric tilt boundary of iron, ISIJ Int. 48 (2008) 1582–1591.
[29] Y. Shibuta, S. Takamoto, T. Suzuki, Dependence of the grain boundary energy on the alloy composition in the bcc iron-chromium alloy: a molecular dynamics study, Comput. Mater. Sci. 44 (2009) 1025–1029.
[30] T. Hirouchi, T. Tsuru, Y. Shibutani, Grain growth prediction with inclination dependence of <1 1 0 > tilt grain boundary using multi-phase-field model with penalty for multiple junctions, Comput. Mater. Sci. 53 (2012) 474–482.
[31] H.-K. Kim, S.G. Kim, W. Dong, I. Steinbach, B.-J. Lee, Phase-field modeling for 3D grain growth based on a grain boundary energy database, Model. Simulat. Mater. Sci. Eng. 22 (2014) 034004.
[32] J.J. Hoyt, M. Asta, A. Karma, Method for computing the anisotropy of the solid-liquid interfacial free energy, Phys. Rev. Lett. 86 (2001) 5530–5533.
[33] D.Y. Sun, M. Asta, J.J. Hoyt, Crystal-melt interfacial free energies and mobilities in fcc and bcc Fe, Phys. Rev. B 69 (2004) 174103.
[34] Y. Watanabe, Y. Shibuta, T. Suzuki, A molecular dynamics study of thermodynamic and kinetic properties of solid-liquid interface for bcc iron, ISIJ Int. 50 (2010) 1158–1164.
[35] Y. Shibuta, K. Oguchi, M. Ohno, Million-atom molecular dynamics simulation on spontaneous evolution of anisotropy in solid nucleus during solidification of iron, Scripta Mater. 86 (2014) 20–23.
[36] F.H. Streitz, J.N. Glosli, M.V. Patel, Beyond finite-size scaling in solidification simulations, Phys. Rev. Lett. 96 (2006) 225701.
[37] Y. Shibuta, K. Oguchi, T. Takaki, M. Ohno, Homogeneous nucleation and microstructure evolution in million-atom molecular dynamics simulation, Sci. Rep. 5 (2015) 13534.
[38] Y. Shibuta, S. Sakane, T. Takaki, M. Ohno, Submicrometer-scale molecular dynamics simulation of nucleation and solidification from undercooled melt: linkage between empirical interpretation and atomistic nature, Acta Mater. 105 (2016) 328–337.
[39] Z.Y. Hou, K.J. Dong, Z.A. Tian, R.S. Liu, Z. Wang, J.G. Wang, Cooling rate dependence of solidification for liquid aluminium: a large-scale molecular dynamics simulation study, Phys. Chem. Chem. Phys. 18 (2016) 17461–17469.
[40] Y. Shibuta, S. Sakane, E. Miyoshi, S. Okita, T. Takaki, M. Ohno, Heterogeneity in homogeneous nucleation from billion-atom molecular dynamics simulation of solidification of pure metal, Nat. Commun. 8 (2017) 10.
[41] Z. Fan, Y. Wu, X. Zhao, Y. Lu, Simulation of polycrystalline structure with Voronoi diagram in Laguerre geometry based on random closed packing of spheres, Comput. Mater. Sci. 29 (2004) 301–308.
[42] S. Falco, J. Jiang, F. De Cola, N. Petrinic, Generation of 3D polycrystalline microstructures with a conditioned Laguerre-Voronoi tessellation technique, Comput. Mater. Sci. 136 (2017) 20–28.
[43] S. Okita, Y. Shibuta, Grain growth in large-scale molecular dynamics simulation: linkage between atomic configuration and von Neumann-Mullins relation, ISIJ Int. 56 (2016) 2199–2207.
[44] S. Okita, W. Verestek, S. Sakane, T. Takaki, M. Ohno, Y. Shibuta, Molecular dynamics simulations investigating consecutive nucleation, solidification and grain growth in a twelve-million-atom Fe-system, J. Cryst. Growth 474 (2017) 140–145.
[45] J. von Neumann, in: C. Herring (Ed.), Metal Interfaces, American Society for Metals, Cleveland, 1952, pp. 108–110.
[46] W.W. Mullins, Two–dimensional motion of idealized grain boundaries, J. Appl. Phys. 27 (1956) 900–904.
[47] R.D. MacPherson, D.J. Srolovitz, The von Neumann relation generalized to coarsening of three-dimensional microstructures, Nature 446 (2007) 1053–1055.
[48] E.A. Holm, S.M. Foiles, How grain growth stops: a mechanism for grain-growth stagnation in pure materials, Science 328 (2010) 1138–1141.
[49] M.W. Finnis, J.E. Sinclair, A simple empirical N-body potential for transition metals, Philos. Mag. a 50 (1984) 45–55.
[50] H.J.C. Berendsen, J.P.M. Postma, W.F. van Gunsteren, A. DiNola, J.R. Haak, Molecular dynamics with coupling to an external bath, J. Chem. Phys. 81 (1984) 3684–3690.
[51] H.C. Andersen, Molecular dynamics simulations at constant pressure and/or temperature, J. Chem. Phys. 72 (1980) 2384–2393.
[52] Y. Shibuta, T. Suzuki, A molecular dynamics study of the phase transition in bcc metal nanoparticles, J. Chem. Phys. 129 (2008) 144102.
[53] J.K. Mackenzie, Second paper on statistics associated with the random disorientation of cubes, Biometrika 45 (1958) 229–240.
[54] K. Oguchi, Y. Shibuta, T. Suzuki, Accelerating molecular dynamics simulation performed on GPU, J. Jpn. Inst. Met 76 (2012) 462–467.
[55] M.P. Allen, D.J. Tildesley, Computer Simulation of Liquids, Oxford University Press, Oxford, 1989.
[56] M. Hillert, On the theory of normal and abnormal grain growth, Acta Metall. 13 (1965) 227–238.
[57] P. Feltham, Grain growth in metals, Acta Metall. 5 (1957) 97–105.
[58] E. Miyoshi, T. Takaki, Multi-phase-field study of the effects of anisotropic grain-boundary properties on polycrystalline grain growth, J. Cryst. Growth 474 (2017) 160–165.
[59] A. Kazaryan, Y. Wang, S.A. Dregia, B.R. Patton, Grain growth in anisotropic systems: comparison of effects of energy and mobility, Acta Mater. 50 (2002) 2491–2502.
[60] P.R. Rios, T.G. Dalpian, V.S. Brandão, J.A. Castro, A.C.L. Oliveira, Comparison of analytical grain size distributions with three-dimensional computer simulations and experimental data, Scripta Mater. 54 (2006) 1633–1637.
[61] R. Darvishi Kamachali, A. Abbondandolo, K.F. Siburg, I. Steinbach, Geometrical grounds of mean field solutions for normal grain growth, Acta Mater. 90 (2015) 252–258.
[62] C. Deng, C.A. Schuh, Diffusive-to-ballistic transition in grain boundary motion studied by atomistic simulations, Phys. Rev. B 84 (2011) 214102.
[63] F. Ulomek, V. Mohles, Separating grain boundary migration mechanisms in molecular dynamics simulations, Acta Mater. 103 (2016) 424–432.
[64] E. Miyoshi, T. Takaki, Y. Shibuta, M. Ohno, Multi-phase-field grain growth simulations starting from molecular dynamics-generated polycrystalline structures, in: The Proceedings of the Computational Mechanics Conference, 2017.30, 2017, p. 55, https://doi.org/10.1299/jsmecmd.2017.30.055.